Turbulence Modeling for Engineering Flows

By Florian R. Menter
Research and Development Fellow
ANSYS, Inc.

Turbulence is arguably the most challenging area in fluid dynamics and the most limiting factor in accurate computer simulation of engineering flows. It constitutes a classical multi-scale problem, which is far beyond human intuitive understanding and beyond resolution capabilities of even the most powerful modern parallel computers (for any foreseeable future). Turbulence has been described by Nobel-prize winning physicist Richard Feynman as the "most important unresolved problem in classical physics." An even more pronounced quote is associated to Werner Heisenberg: "When I meet God, I am going to ask him two questions: Why relativity? And why turbulence? I really believe he will have an answer for the first."

From a more pragmatic standpoint, however, one could argue that a complete understanding of turbulence is not required (and there is actually no indication that humans can comprehend complex nonlinear problems), but a sufficiently accurate solution of the underlying equations (better, a general method for achieving those) would suffice. Such numerical methods exist and allow a direct numerical simulation (DNS) of Navier–Stokes equations for all turbulence scales in space and time. However, due to the inherent scaling laws of turbulence, DNS can be applied only to very low Reynolds (Re) numbers and very simple and limited geometries. The numerical effort for DNS scales with Re^3, and with technical Re numbers in the range of 10^4 to 10^9, practically no numerical solution for flows of interest to engineers can be obtained. Turbulence modeling is the attempt to develop approximate formulations that, despite our incomplete understanding and limited computational resources, allow engineers to obtain approximate solutions for their pressing technological applications. When dealing with turbulence models, keep in mind that they often need to bridge a gap of many orders of magnitude in computing power relative to DNS. The order of CPU reduction of RANS methods relative to DNS for technical applications is astronomic (easily reaching 10^{10} and more) — such models, therefore, are not simply "models," but they alter and redefine the equations solved. Industrial users are often (understandably) disturbed by RANS-related inaccuracies in their CFD solution relative to data. Considering the above challenge, such differences cannot always be avoided. Finally, not all differences between numerical results and experimental data are automatically a result of turbulence modeling; there are many other sources of error (for example, Roache 1989) that should be considered before casting a judgment on a model.

Industrial CFD codes have to cover a wide range of applications from aerodynamics to internal flows, flows with heat and mass transfer to inherently unsteady applications. There are numerous areas of turbulence interaction with other physical effects, like combustion or acoustics. Obviously, no single model (or modeling approach) can cover all such applications, and numerous modeling concepts need to be developed. On the other hand, it would not be appropriate to simply program an indiscriminate number of models into industrial CFD codes, as it would have severe negative effects on the user community. The first is that most models published are not "industrial-strength," meaning they have severe weaknesses that prevent efficient use for complex problems. The most

prominent limitation is numerical robustness, as many new models are applied only to generic test cases with relatively simple geometries and high-quality grids. When faced with less-optimal conditions, they often pose severe challenges to the solver and, in many cases, lead to numerical instabilities. Most models based on the low-Re ε-equations fall into this category. Furthermore, models often feature many complex nonlinear terms, which are designed to resolve a very specific problem in generic tests, but the side effects of such terms in complex flows are not sufficiently considered. From a coding standpoint, it is desirable to limit the number of models, as otherwise implementation quality will suffer and the user cannot rely on the correct and optimal programming of equations. Support teams need to understand turbulence models to ensure proper response to customer problems in a short timeframe. An oversupply of models severely limits the engineering team's ability to properly help customers and supply best-practice advice. Finally, the different models and submodels have to work properly in combination (for example, turbulence and transition, etc.). For these reasons, it is necessary to provide a limited number of preselected models that are:

- Well understood and tested
- Correctly implemented and documented
- Accurate for certain classes of flows
- Robust even for nonoptimal grids
- Interoperable with other models and submodels
- Supported by test cases

The interplay of technology and implementation aspects becomes even more pronounced for scale-resolving simulation (SRS) methods like scale-adaptive simulation (SAS) (Menter and Egorov 2010, Egorov et al. 2010), detached eddy simulation (DES) (Spalart 2000, Spalart et al. 2006, Strelets 2001), or large eddy simulation (LES) (Smagorinsky 1963), in which the numerical scheme has a direct impact on model accuracy. For such models, it has to be assured that the numerical method selected matches accuracy requirements of the underlying turbulence model.

This paper focuses on the industrial formulation and application of turbulence models. These notes, therefore, do not attempt to provide a comprehensive overview of turbulence modeling theory; instead, they outline the current status of models used in industrial codes as well as methods with potential for the next generation of industrial applications. The material is closely aligned with the author's line of work. For basic coverage of turbulence modeling, refer to textbooks such as Durbin and Reif (2001) or Wilcox (2006).

Reynolds-Averaged Navier–Stokes Modeling

GENERAL ASPECTS

Osborne Reynolds proposed an averaging concept for the Navier–Stokes equations that significantly reduces the complexity of simulating turbulent flows. The resulting Reynolds-averaged Navier–Stokes (RANS) equations are formulated in terms of the (time-) averaged flow field (velocity field, pressure, density and temperature). Turbulence fluctuations are eliminated by this process, and the equations become amenable to computational fluid dynamics (CFD) on today's desktop computers. However, the price for this simplification lies in the additional Reynolds stress tensor that appears in the RANS equation as a result of the nonlinear terms of the underlying Navier–Stokes equations. (See, for example, Wilcox 2006.) These terms are unknown, and the equations are therefore not "closed," meaning there are more unknowns than equations. The task of RANS turbulence modeling is to close the equations and provide a link between the mean velocity field and Reynolds stresses. Within the RANS concept, all turbulence is modeled, meaning the computer spends effort on only the computation of the mean flow, and no attempt is made to resolve turbulent structures in time and space. As stated, RANS models have to bridge many orders of magnitude in computing power and, therefore, will not always produce results with a narrow error margin. Purists may consider this a principle failure in technology and turn to more "scientific" methods like large eddy simulation, as has been the case in the last decades with most

academic engineering institutions. However, this does not give credit to the success of RANS, on which basically all of today's industrial CFD simulations are based. RANS models, if selected and applied properly, offer engineers a highly attractive balance between computing resources and accuracy required for most industrial applications. While many have projected LES would substitute RANS models gradually as more CPU power becomes available, there is no indication of this change happening on a large scale. Many companies face more pressing needs, such as including larger parts of their geometry, by moving from components to systems, or accounting for additional physical effects (like fluid–structure interaction, etc.) in their simulations. (See, for example, Pope 1999.) The fact that many companies frequently follow this route, instead of investing the additional CPU power into methods like LES, is further testimony to the trust they place in employed RANS methods. While there is no question that scale-resolving simulation methods will become more dominant in the future, it is worthwhile keeping a foot in the door of RANS modeling, as any advancement in this area can have a large impact and can improve a wide range of engineering flow simulation.

NEAR-WALL TREATMENT

The success of RANS models is mostly manifested by the accuracy achieved in computation of wall-bounded flows. Virtually all turbulence models can predict zero-pressure gradient boundary layers, thereby already covering a major application sector. While there are many applications in which more subtle capabilities are required from a model, many technical devices are dominated by flat surfaces with flow separation dictated by geometric discontinuities like corners and sharp edges. These types of applications have been well covered by basic two-equation models and, to a degree, explain the long-term success of the classical k-ε model with wall functions. However, increased accuracy demands and more complex shapes have resulted in a need for turbulence models that are able to predict flow separation from smooth surfaces under adverse pressure gradients as they appear in aerodynamics or internal diffuser-like flows. Such accuracy requirements are typically linked to the ability of models to allow for integration to the wall. Such "low-Reynolds numbers," or more accurately viscous sublayer models (VSM), eliminate much of the resolution problems imposed by wall functions. Modern CFD codes feature models that automatically adapt to the near-wall resolution and smoothly blend between wall functions and VSM as the grid is refined (Menter and Esch 2001, Kim et al. 2002, Kalitzin et al. 2005, Popovac and Hanjalic 2007). In the author's opinion, standard wall functions with limitations like "the grid should not be refined beyond a y^+ of 30, etc." should be abandoned in favor of y^+-insensitive wall formulations. In principle, any model that imposes lower limits on grid resolution is highly problematic as it does not allow for a distinction between numerical and modeling errors, which can only be obtained under systematic mesh refinement.

Figure 1 shows wall shear stress and wall heat transfer simulations for a flat plate on five vastly different grids (y^+ = 0.17, 0.81, 4.3, 11.6, 20.8, 41.6) using a y^+-insensitive wall formulation in combination with the ω-equation. Despite the large differences in near-wall spacing, computed wall shear-stress and Stanton numbers vary by less than 5 percent, and all solutions follow the experimental data. As a result, such a wall formulation can significantly improve the predictive accuracy for general industrial applications, as user influence via grid generation is drastically reduced.

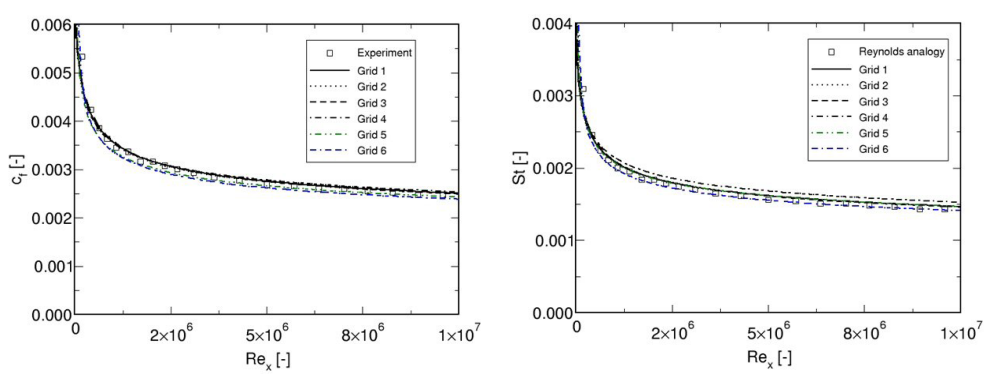

Figure 1. *Wall shear stress (c_f) and wall heat transfer (St) coefficients for flat plate boundary layer on different numerical grids (y^+ = 0.17, 0.81, 4.3, 11.6, 20.8, 41.6)*

THE SCALE EQUATION : ε- VS. ω-EQUATION

While much of the discussion in RANS modeling has focused on the comparison of eddy viscosity vs. Reynolds stress models (RSM), the impact of the scale equation, particularly for wall boundary layers, is similarly important. While the ε-equation has been successfully applied to many industrial CFD simulations, often in combination with wall functions, the author believes that the ω-equation offers a more accurate and robust modeling framework for boundary layers. The deficiencies of the ε-equation in this respect are well known, namely a much-too weak response to adverse pressure gradients and, thereby, a strong tendency to miss or under-predict separation. This is a serious issue, as it results in overly optimistic loss/stall predictions, leading the design engineer to believe the flow is attached when it is already in a range with large separation-related losses. Furthermore, the ε-equation has posed major challenges to be extended for integration through the viscous sublayer. While many viscous sublayer model (VSM) extensions have been developed for the ε-equation, they are typically difficult to converge and can even lead to multiple solutions already for simple flows (laminarization). A remedy is the use of a two-layer formulation (See Rodi 1991.), which allows integration to the wall and extension to a y^+-insensitive wall treatment. This formulation is a substantial improvement compared to the use of wall functions — but not as accurate as the near-wall formulation of the ω-equation, especially for flows with adverse pressure gradients.

In more recent years (Durbin 1995), the concept of elliptic relaxation was introduced to the ε-equation framework to avoid the need for damping functions in the viscous sublayer region. On closer inspection one finds that the *k*-ω model has a built-in elliptic relaxation. Near the wall, the ω-equation reduces to (for constant viscosity μ):

$$\mu \frac{\partial^2 \omega}{\partial x_j^2} = \beta \rho \omega^2$$

This equation, in combination with the values specified for ω at the wall, efficiently communicates the wall presence to the flow in the near-wall region without a need for additional transport equations or damping functions. This makes the ω-equation a highly attractive and robust modeling framework.

On the other hand, the ω-equation has shown a disturbing sensitivity to freestream values imposed for ω at the boundary layer edge (through the inlet values) (Menter 1992, 2009). This has led the author to develop a model formulation that combines the advantages of the ε- and ω-equation (Menter, 1994). The resulting baseline (BSL) model serves today as the basis of many turbulence models, such as the SST model, ω-equation-based RSM or DES models (Strelets, 2001). The SST model has particularly gained widespread usage in aerodynamics and general CFD applications since its introduction (Menter 1994, Menter 2009). In addition, the ω-equation is well suited for combining with the laminar-turbulent transition modeling (Menter et al. 2006, Langtry and Menter 2009). Figure 2 shows the central role the BSL ω-equation plays in an integrated modeling approach, in which all different elements can be combined. By combining all different elements under one scale equation, the impact of different additions on the solution can be checked systematically, without a need for changing several aspects of the model. Finally, selecting an optimal scale equation does not prevent the inclusion of other modeling concepts, as terms can easily be transformed from one equation to another.

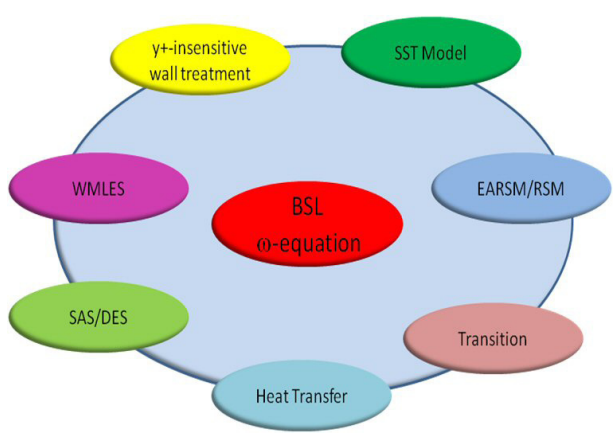

Figure 2. *ω-equation-based modeling concept*

Figure 3 shows a comparison of model predictions for the flow around an NACA 4412 airfoil (Coles and Wadcock, 1979), (α=13.87, Re=1.5x10^6), at high angle of attack with some more-popular eddy viscosity models. Visibly, the SST model provides the best agreement against experimental data. Similar comparisons between models are observed for other flows of the same nature. No *k*-ε solutions are included in this figure, as none of the models is able to capture flow separation observed in the experiment. Flow separation under pressure gradients is present in many technical devices, and an accurate representation is essential for a reliable CFD simulation. The ability to predict separation lines accurately has made the SST model popular in and beyond the aeronautics application area.

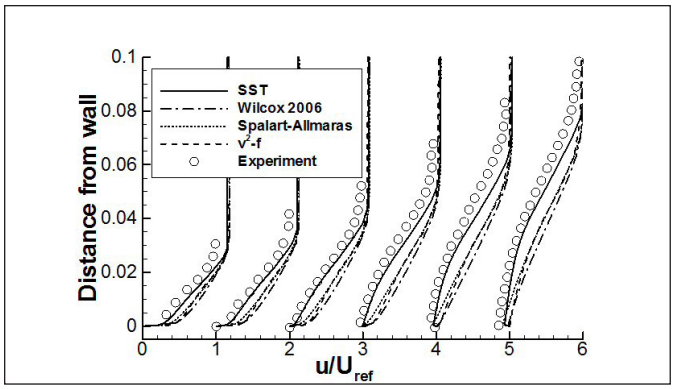

Figure 3. *Comparison of velocity profiles for NACA 4412 airfoil (α=13.87°, Re=1.5x10^6) using different turbulence models*

In a more severe test, the SST model was applied to test cases of the 2003 AIAA Drag Prediction Workshop (Langtry et al. 2004). The goal of the workshop was to evaluate if current turbulence models and CFD methods allow prediction of increased drag caused by installation of an engine nacelle. The two configurations tested are shown in Figure 4. The models have been designed and tested experimentally by DLR (Broderson and Stürmer, 2001). Figure 5 shows the drag polars (lift vs. drag as a function of angle of attack) predicted with ANSYS® CFX® software for both configurations using the SST model. Agreement with the data is very close and clearly displays the offset in drag caused by addition of the pylon-nacelle. The small but systematic difference for the wing-body-nacelle-pylon (WBNP) case is most likely a result of the relatively low mesh resolution of around 12 million cells. Considering that drag has a small value near cruise conditions (one order of magnitude less than lift), this example demonstrates the accuracy that can be achieved with ω-equation-based RANS models for wall-bounded flows.

Figure 4. *Geometries of DLR-F6 models for AIAA Drag Prediction Workshop*
(Courtesy DLR Braunschweig.)

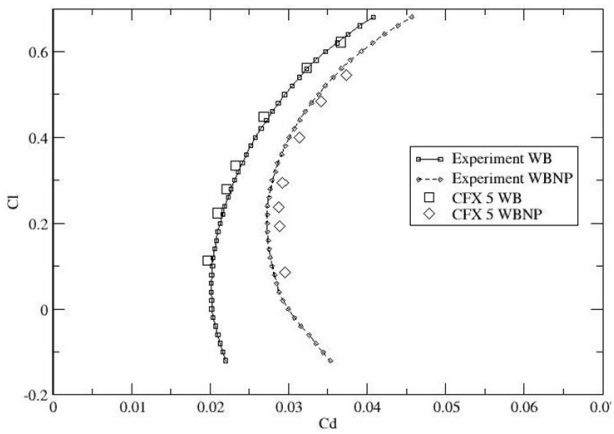

Figure 5. *Drag polars for WB and WBNP test case*

TRANSITION MODEL FORMULATION

For many decades, modeling of laminar–turbulent transition in boundary layers has proven one of the most challenging tasks in CFD. While many industrial flows are in the range of $10^4<Re<10^6$, meaning in regimes where significant portions of the boundary layers can be laminar, there was simply no reliable way of including these effects even to first order in general-purpose CFD codes. Laminar–turbulent transition affects many aspects of industrial flows. The main effect is that the skin friction in the laminar portion of the boundary layer is substantially lower than in the turbulent part. This also affects heat transfer predictions strongly with much-reduced heat transfer in the laminar zone. For applications under adverse pressure gradients, laminar separation bubbles with turbulent reattachment can appear. They can have a significant effect on the aerodynamic characteristics of device, as observed for wind turbine blades or compressor flows.

Recently, a new transition model compatible with the SST model that allows the inclusion of such effects into general CFD simulations has been developed (Menter et al. 2006, Langtry and Menter 2009). The model solves two additional transport equations (γ-Re_Θ model) and incorporates experimental correlations to trigger the transition onset. The model formulation is strictly local and, therefore, fully compatible with modern general-purpose CFD codes. Note that there is no need for the user to specify boundary layer thickness as incorrectly described by Malan et al. (2009). Discussion of the model equations is beyond the scope of this article and, therefore, is not presented here but can be found in the references. Another innovative model with similar functionality is that of Walters and Cokljat (2008).

The γ-Re_Θ transition model has been validated against a wide range of experimental data and is used today successfully in many industrial CFD simulations. The application range covers turbomachinery blades, wind turbines and racing cars as well as the design of sailing yachts for the Americas Cup.

The T3C test cases consist of a flat plate with favorable and adverse pressure gradients imposed by the opposite converging/diverging walls. The wind tunnel Reynolds number was varied for the four cases (T3C5, T3C3, T3C2, T3C4), thus moving the transition location from favorable pressure at the beginning of the plate to adverse pressure gradient at the end. The cases are used to demonstrate the transition model's ability to predict transition under the influence of various pressure gradients. Figure 6 details the results for the pressure gradient cases. The effect of the pressure gradient on the transition length is clearly visible with favorable pressure gradients increasing the transition length and adverse pressure gradients reducing it. For the T3C4 case, the laminar boundary layer actually separates and undergoes separation-induced transition. Separation-induced transition turns out to be one of the most important and most frequently encountered transition mechanisms in technical flows; it is well covered by the model.

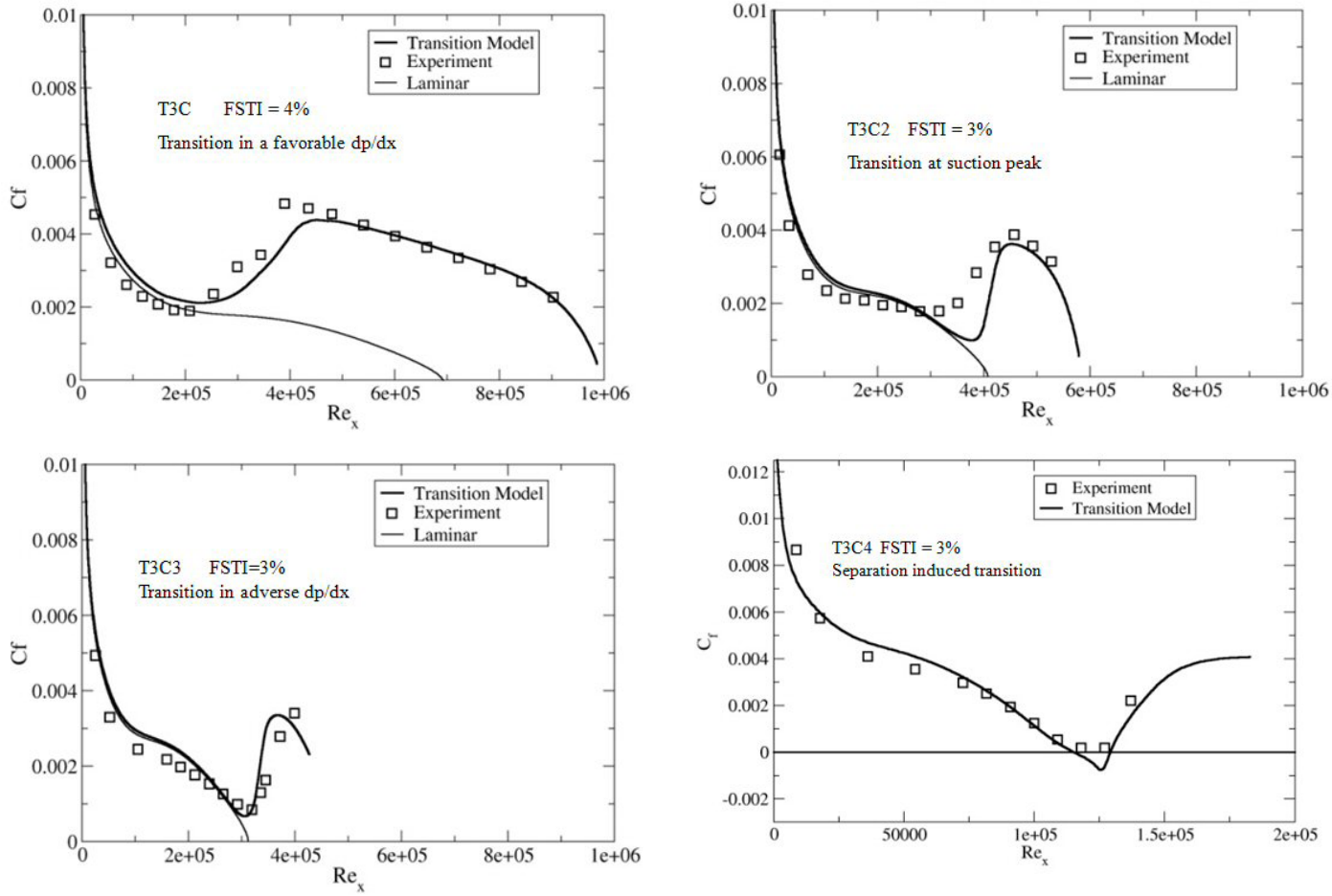

Figure 6. *Results for flat plate test cases in which variation of the tunnel Reynolds number causes transition to occur in different pressure gradients (dp/dx)*

A very demanding test case for the model is the McDonald Douglas 30P-30N flap configuration, originally a test case for the High-Lift Workshop/CFD Challenge that was held at the NASA Langley Research Center in 1993 (Klausmeyer and Lin 1997). It is a complex test case for a transition model because of the large changes in pressure gradient and varying local freestream turbulence intensity around different lifting surfaces. The comparison presented in this paper uses the Reynolds number Re=9x10^6 and an angle of attack AoA = 8°. The freestream conditions for *k* and ω were selected to match the transition location at the slat's suction side. The other transition locations are an outcome of the simulation.

A contour plot of the predicted turbulence intensity around the flap is shown in Figure 7. Also indicated are various transition locations that were measured in the experiment (Exp.) as well as locations predicted by the present transition model (CFD). In the computations, the onset of transition was judged as the locations where the skin friction first started to increase due to production of turbulent kinetic energy in the boundary layer. In general, the agreement between measured and predicted transition locations is very good. The largest error was observed on the lower surface of the main element where the predicted transition location was too far downstream by approximately 6 percent of the cruise-airfoil chord.

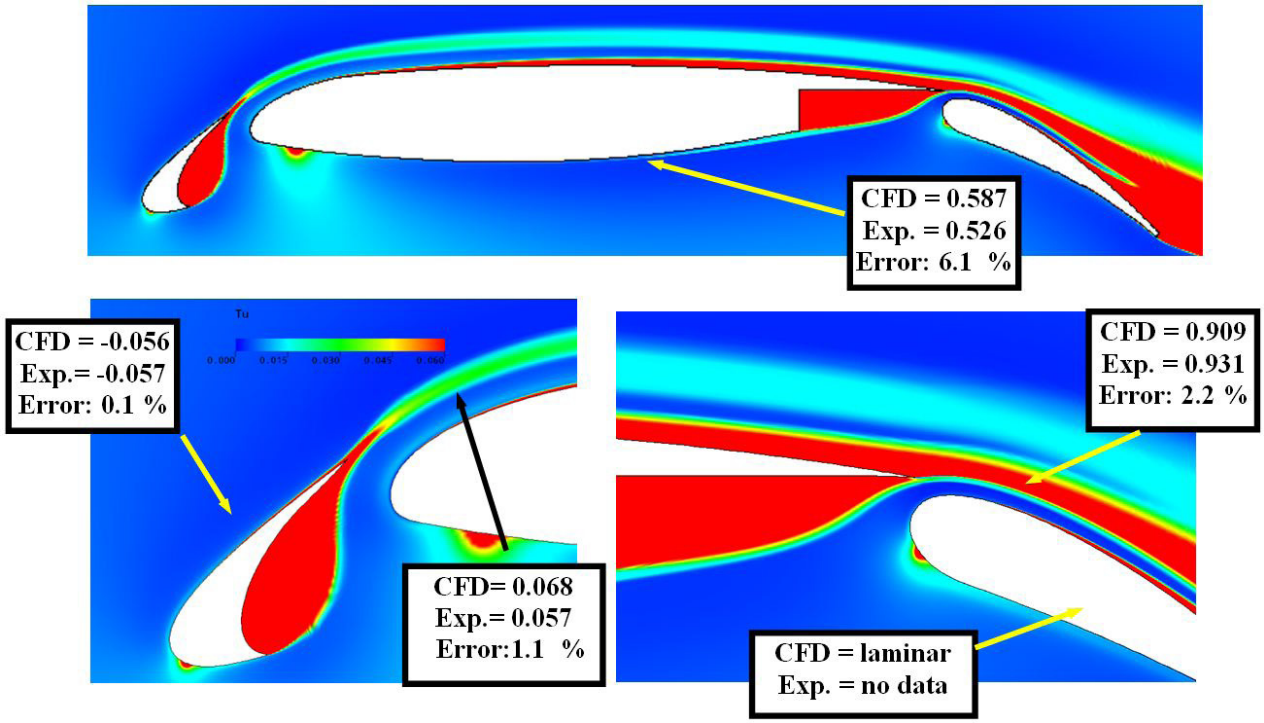

Figure 7. *Contour of turbulence intensity (Tu) around the McDonald Douglas 30P-30N flap as well as measured (Exp.) and predicted (CFD) transition locations (x/c) as a function of the cruise-airfoil chord (c= 0.5588 m). Also indicated is relative error between experiment and predictions.*

The Pratt and Whitney PAK-B low pressure turbine blade is particularly interesting because it has a loading profile similar to rotors found in many modern aircraft engines (Dorney et al. 2000, Huang et al. 2003). The low-pressure rotors on modern aircraft engines are extremely challenging flow fields. In many cases, the transition occurs in the free shear layer of a separation bubble on the suction side (Mayle 1991). The onset of transition in the free shear layer determines whether or not the separation bubble will reattach as a turbulent boundary layer and, ultimately, whether or not the blade will stall.

The experiments were performed at the design incidence angle for Reynolds numbers of 50,000, 75,000, and 100,000 based on inlet velocity and axial chord length, with turbulence intensities of 0.08 percent, 2.35 percent and 6.0 percent (which corresponded to values of 0.08 percent, 1.6 percent and 2.85 percent, respectively, at the leading edge of the blade).

The computed pressure coefficient distributions for various Reynolds numbers and freestream turbulence intensities compared to experimental data are shown in Figure 8. Comparisons are organized such that the horizontal axis denotes the Reynolds number whereas the vertical axis corresponds to the freestream turbulence intensity of the specific case. The most important feature of this test case is the extent of the separation bubble on the suction side, characterized by the plateau in pressure distribution. The size of the separation bubble is actually a complex function of the Reynolds number and the freestream turbulence value. As the Reynolds number or freestream turbulence decrease, the size of the separation and, hence, the pressure plateau increase. The computations with the transition model compare well with experimental data for all of the cases considered, illustrating the ability of the model to capture the effects of Reynolds number and turbulence intensity variations on the size of a laminar separation bubble and subsequent turbulent reattachment.

In Menter et al. 2006 and Langtry and Menter 2009, a large number of additional test cases can be found for this model. Though they cannot be shown due to space limitations, they demonstrate that the model is suitable for

a wide range of technical flows. The model is currently under reconstruction to simplify the formulation and to include additional physical effects like crossflow instability or hypersonic flow transition.

Transition models can only be combined with turbulence models that do not mimic transitional behavior due to their VSM formulation. Otherwise, the interference of both formulations would result in an unpredictable behavior. The ω-equation-based transition models are the most suitable choice there.

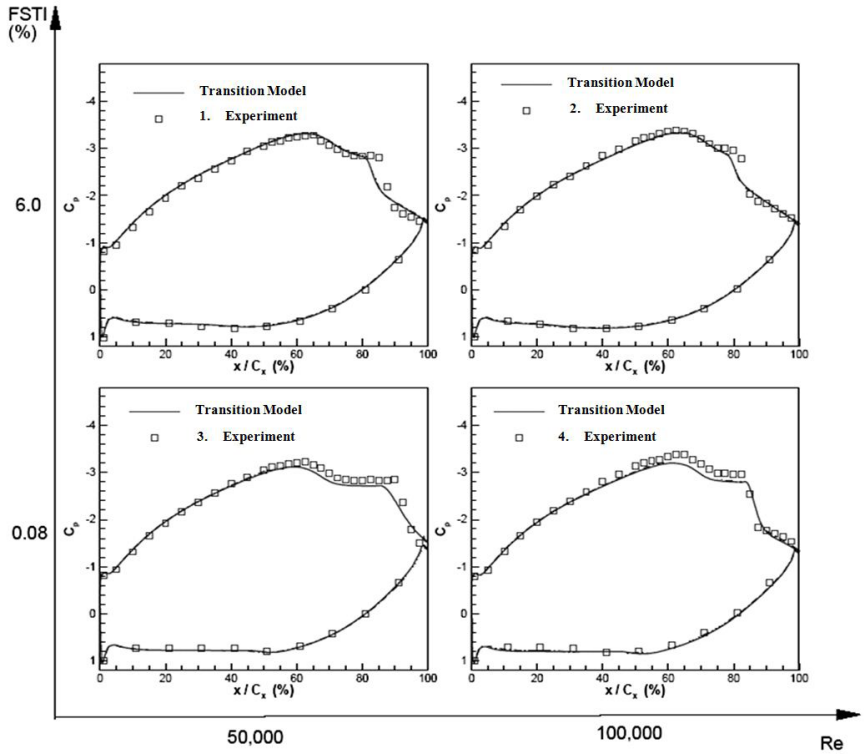

Figure 8: *Blade loading for Pak-B low-pressure turbine at various freestream turbulence intensities (FSTI) and Reynolds numbers (Re)*

BEYOND EDDY VISCOSITY

Eddy viscosity models are very attractive as they offer well-calibrated performance at relatively low computational costs, due to their robust and straight-forward integration into CFD codes. However, there are situations in which eddy viscosity models cannot provide the information required to accurately compute the physical effects at hand. The most classic example is flows with strong swirl or streamline curvature. Another class of flows in which eddy viscosity models may fail is flows in which secondary motion driven by turbulence anisotropies is important. Historically, the strategy in such cases has been to move on to Reynolds stress models (for example, Wilcox 2006), which requires solving one transport equation for each component of the Reynolds stress tensor (six equations due to the symmetry of the tensor plus an equation for the scale equation). For a long time, RSMs have been considered the natural next level of modeling beyond eddy viscosity models, but in general they have never quite lived up to this standard. The main limitation has frequently been due to reduced numerical robustness, especially if the equations need to be integrated through the viscous sublayer. Successful systematic RSM applications have, therefore, mostly been to flows in which wall boundary layers are not central or where a wall-function resolution is sufficient. This limitation can be partly alleviated by combining RSM with the ω-equation, which also provides a more-robust framework for boundary layer integration.

An intermediate formulation between eddy viscosity and RSM is explicit algebraic RSM (EARSM) in which RSM transport equations are reduced to algebraic form under equilibrium assumptions (Rodi 1976, Wallin and

Johansson 2000). These models naturally account for effects of anisotropy while still requiring only the solution of two transport equations. There are also extensions that allow inclusion of curvature and rotation effects in a way consistent with EARSM formulation. While no anisotropic model will be as robust as linear eddy viscosity models, EARSMs appear to be more robust than RSM, even for fine near-wall meshes.

Figure 9 shows the effect of including anisotropy into the simulation for a wing-body junction. In this case, linear eddy viscosity models like the SST or Spalart–Allamars model tend to overpredict the size of the corner separation relative to experimental data. The WJ-based BSL-EARSM (Menter et al. 2009) does give improved predictions with a reduced size of the corner separation bubble. This effect can be more pronounced for cases with lower aspect ratios, such as turbomachinery blades or low-aspect ratio diffusers.

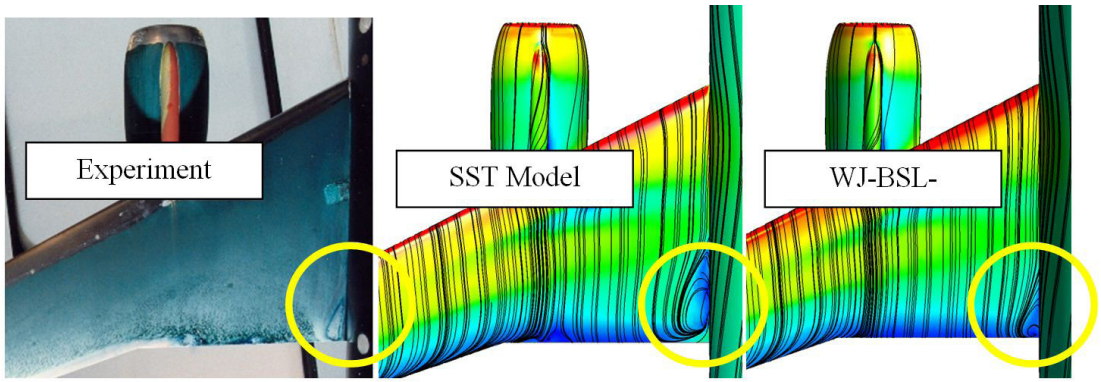

Figure 9. *Separation zone at wing–fuselage junction (left). Oil film visualization in the experiment against experimental data; yellow circle shows corner separation*

Scale-Resolving Simulation

While today's CFD simulations are based mainly on RANS models, certain classes of flows are better covered by models in which at least a portion of the turbulence spectrum is resolved in at least a portion of the numerical domain. Such methods are termed scale-resolving simulation (SRS) models.

The argument has been made that RANS models have shown their strength essentially for wall-bounded flows, in which the calibration according to the law-of-the-wall provides a very sound foundation for further refinement. For free-shear flows, the situation is much less uniform. There is a wide variety of such flows, ranging from simple self-similar flows like jets, mixing layers and wakes to impinging flows, flows with strong swirl, massively separated flows, and many more. Considering that RANS models typically have limitations covering the most basic self-similar free-shear flows with one set of constants, there is little hope that even the most advanced RSM will eventually be able to provide a reliable foundation for all such flows. On the other hand, for free-shear flows, it is typically much easier to resolve the largest turbulent scales, as they are of the order of the thickness of the shear layer. In contrast, for wall boundary layers, the turbulence length scale becomes very small relative to boundary layer thickness near the wall (increasingly so with increased Re number). This poses severe limitations for LES models, as the computational effort required is still far from today's available computing power. For this reason, hybrid models are under development, in which large eddies are only resolved away from walls and the wall boundary layers are covered by a RANS model. For an overview of SRS modeling concepts, see Fröhlich and von Terzi 2008.

LARGE EDDY SIMULATION

Large eddy simulation, the first SRS method, has been under development for more than four decades starting from the early work of Smagorinsky 1963. In all this time, LES has never lived up to the expectations that it could eventually replace RANS models on a grand scale, despite the substantial effort invested into this technology. The main limitation results from the high resolution demands for wall-bounded flows, an issue never truly confronted in its entirety by the LES community. For this reason, classical LES has largely remained a research tool, with some sporadic industrial applications to flows not much affected by wall boundary layers like the central combustion section of combustion chambers.

It is instructive to compare the numerical effort required for a RANS and LES simulation of the flow over a relatively limited geometry, like a *single* turbine blade in a gas turbine. If the all physical effects — like laminar-turbulent transition and complete 3-D geometry with hub and shroud portions — are included, the estimates are given in Table 1.

	Number of cells	Number of time steps	Number of inner loops per time step	Effort relative to RANS
RANS	~10^6	~10^2-10^3	1	1
LES	~10^9	~10^5	1-10	~10^5-10^6

Table 1: *Estimate of CPU resources for RANS and wall-resolved LES for a single turbine blade*

Of course, details depend on numerics and code etc., but the estimate shows that there are five to six orders of magnitude difference even for this relatively simple geometry. One could argue that this is an extreme case as laminar-turbulent transition needs to be resolved; however, estimates at higher Re numbers as provided by Spalart (2000) are not more favorable. For this reason, pure LES will not become a standard industrial tool for most applications for many decades.

DETACHED EDDY SIMULATION

Detached eddy simulation has been proposed by Spalart and coworkers (Spalart 2000, Spalart et al. 2006, Strelets 2001) to eliminate the main limitation of LES models by using a hybrid formulation that switches between RANS and LES based on the grid resolution provided. By this formulation, the wall boundary layers are entirely covered by the RANS model and the free-shear flow portions are typically computed in LES mode. The formulation is relatively simple and can be built on top of any RANS turbulence model. DES has attained significant attention in the turbulence community, as it allows the inclusion of SRS capabilities into everyday engineering flow simulations.

Within the DES model, the switch between RANS and LES is based on a criterion like:

$$C_{DES}\Delta > L_t \quad \rightarrow \quad RANS \quad ; \quad \Delta = \max\left(\Delta_x, \Delta_y, \Delta_z\right)$$

$$C_{DES}\Delta \leq L_t \quad \rightarrow \quad LES$$

Resolved turbulence is not explicitly introduced into the simulation by an explicit conversion of modeled turbulence to resolved turbulence. The method relies on a sufficiently strong flow instability (such as that observed behind bluff bodies) to produce the resolved content by itself. Obviously, such instability is not always present, and switching the model might simply result in a reduction of the eddy viscosity to an LES formulation without a proper generation of turbulent content. This is the case for wall boundary layers. If the grid is reduced to activate the DES limiter, the eddy viscosity is reduced and the RANS model is no longer functional. In many situations, this can lead to grid-induced separation (GIS) (Menter and Kuntz 2002), in which the boundary layers separate at arbitrary locations based on the grid spacing. To avoid this limitation, the DES concept has been extended to delayed DES (DDES), following the proposal of Menter and Kuntz (2002) to shield the boundary layer from the DES limiter (Shur et al. 2008). This is now the recommended practice, yet the effectiveness depends on details of the shielding function. Functions that provide high protection against GIS can, in turn, limit the model's LES capabilities.

Another important issue is that for free shear flows (in which shielding is not active), the DES limiter is activated much before the grid is actually able to resolve the flow with LES quality. There is approximately an order of magnitude in grid spacing between the activation of the limiter and a sufficient LES resolution. Grids falling in-between these limits produce grey zones, where the flow is neither in RANS nor LES mode. The user of any DES model needs to be keenly aware of such limitations, carefully crafting an appropriate numerical mesh to avoid undefined model behavior. Successful applications of the DES model can be found in Spalart (2000), Spalart et al. (2006), Strelets (2001), Shur (2008), Haase et al. (2009).

SCALE-ADAPTIVE SIMULATION

In recent years, the author's group has developed an alternative method to DES, for which the RANS model is not influenced by the grid spacing (Menter et al. 2010, Egorov et al. 2010). The method is termed scale-adaptive simulation (SAS) and is based on the introduction of the von Karman length scale, L_{vK}, into the turbulence model:

$$L_{vK} = \kappa \left| \frac{U'}{U''} \right|; \quad |U'| = \sqrt{\frac{\partial U_i}{\partial x_j}\frac{\partial U_i}{\partial x_j}}; \quad |U''| = \sqrt{\frac{\partial^2 U_i}{\partial x_k^2}\frac{\partial^2 U_i}{\partial x_j^2}}$$

Unlike DES, SAS models are not affected by GIS or grey zones and can be run on a much wider range of numerical grids. L_{vK} allows the model to adjust to resolved structures in the simulation and automatically reduces the eddy viscosity in such regions to the appropriate LES level if the grid permits. However, if the grid is not of LES resolution, SAS will still produce sensible results, and coarser meshes and/or time steps will fall back to the RANS solution. The SAS model also relies on instability of the flow to generate resolved turbulence like the DES model. In cases in which instability is not present, the model will remain in RANS mode.

Figure 10 shows the flow structures computed by the SST-SAS model for a periodic hill flow. The two pictures represent simulations on the same mesh (~2.5 million nodes) using two different time steps. The time step in the left part of the figure corresponds to a typical LES time step (CFL<1); in the right part, the time step is increased by a factor of four. Further increasing the time step would result in a steady-state RANS solution. Figure 10 also illustrates the terminology scale-adaptive, which allows the model to adjust to the mesh and time step resolution provided, resulting in a continuous variation of the simulation from LES to steady-state RANS. The color in Figure 10 displays the ratio of eddy viscosity to molecular viscosity. In the left part of Figure 10, this ratio is of the order 5 to 10, and in the right part of order 30 to 50. The ability of the model to adjust its eddy viscosity to the resolved scales is unique and cannot be achieved with standard LES models. For Smagorinsky-type models ($\upsilon_1 = (c\Delta)^2 S$), the length scale is fixed by the grid spacing, Δ. For large scales, the strain rate, S, is lower than for small scales. Such a model would, therefore, produce a lower eddy viscosity for large structures than for small ones.

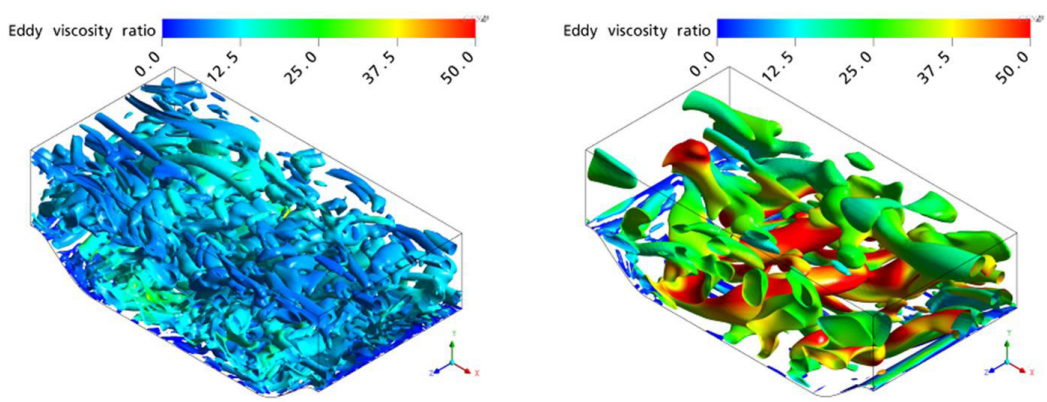

Figure 10. *Turbulent structures for flow over periodic hill with SST-SAS model. Left: small time step (CFL~1); right 4x larger time step; color: ratio of eddy-viscosity to molecular viscosity*

Figure 11 shows the velocity profiles computed with the SAS model using the two different time steps in comparison with reference LES (Temmerman and Leschzner 2001) and SST-RANS solution. Even the large time step leading to the structures seen in the right side of Figure 10 gives a significant improvement in the velocity profiles compared to the steady-state solution. (This case is known to be challenging for RANS models due to its large separation zone and periodic conditions.)

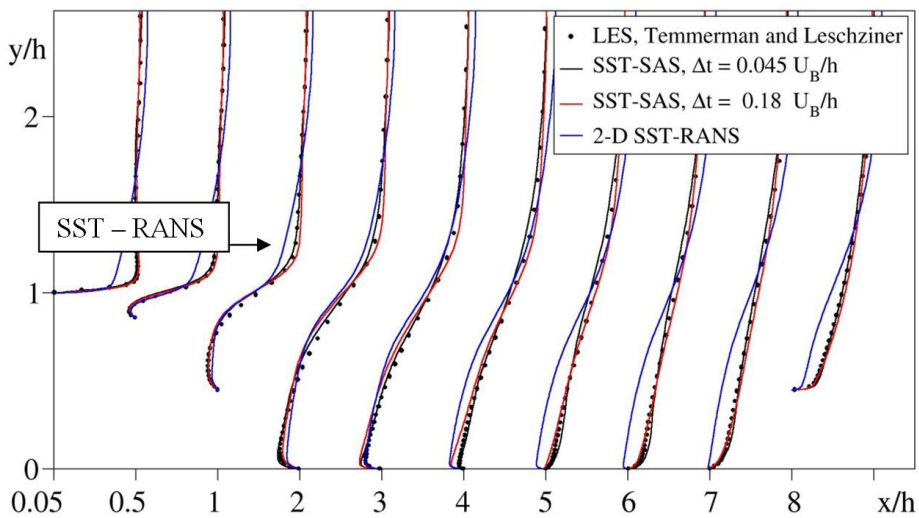

Figure 11. *Velocity profiles for SAS simulations with different time steps for periodic hill flow in comparison with reference LES and SST-RANS solution*

Figure 12 shows SAS simulations over a generic airplane geometry (Laschka et al. 1995). The simulation (Re=2.8x10^6, α=15º) has been carried out on an unstructured mesh with 11x10^6 control volumes. The left part shows the geometry and the turbulent structures produced by the simulation. The right part shows a comparison between experimental data and the time-averaged simulation. The simulation is in good agreement with experimental data (right part of figure).

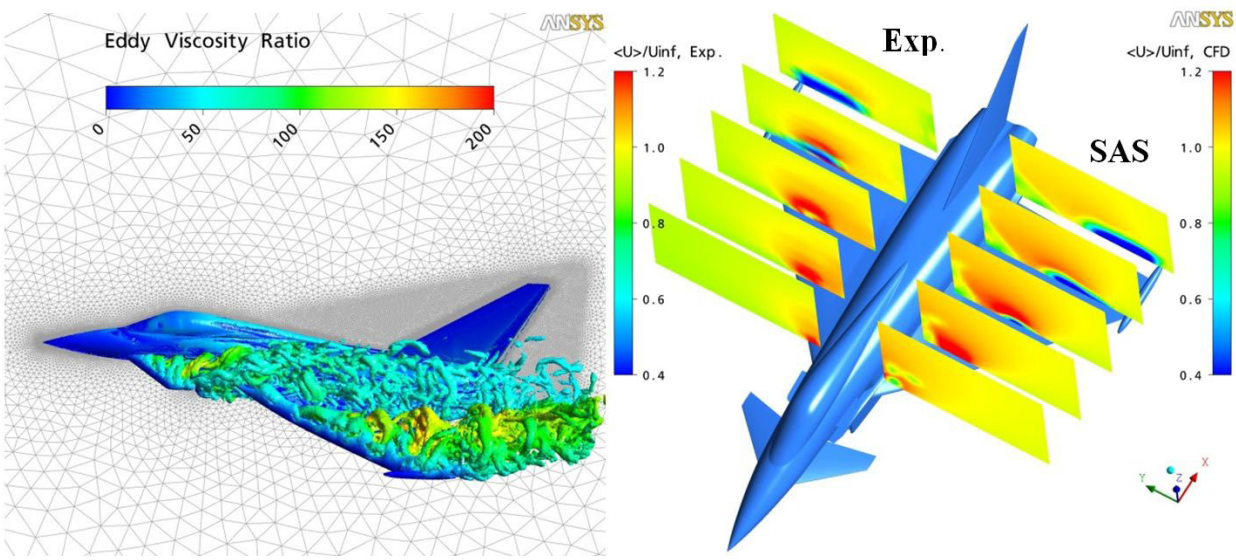

Figure 12. *Flow over generic airplane configuration FA-5. Left: flow structures; right: comparison of experiments and SAS axial flow component* (Geometry and data courtesy EADS Deutschland.)

The SST-SAS model was also applied to the flow in a single-swirl burner investigated experimentally by Schildmacher and Koch (Schildmacher et al. 2000) at ITS (Institut für Thermische Strömungsmaschinen) at the University of Karlsruhe. The ITS burner is a simplified industrial gas turbine combustor.

The flow structures from the SST-SAS computations of the nonreacting and reacting flows at a given instance in time are shown in Figure 13 using the Q-criterion ($Q=\Omega^2-S^2=10^7\ s^{-2}$). Experience shows that classical URANS models are not reliable in predicting the change in flow topology indicated in Figure 13. They typically only predict a single main vortex and miss the intensive mixing caused by the turbulence generated in the unstable regime. This can be seen in more detail in figures 14,15 and 16, showing the radial distributions of statistically averaged velocity and temperature in the mixing zone. Superior accuracy of the SAS results relative to URANS simulation confirms that SAS is a viable method for such a complex flow. This is confirmed by a recent significantly more-detailed evaluation of the SST-SAS model for combustion chamber simulations by Widenhorn et al. (2009).

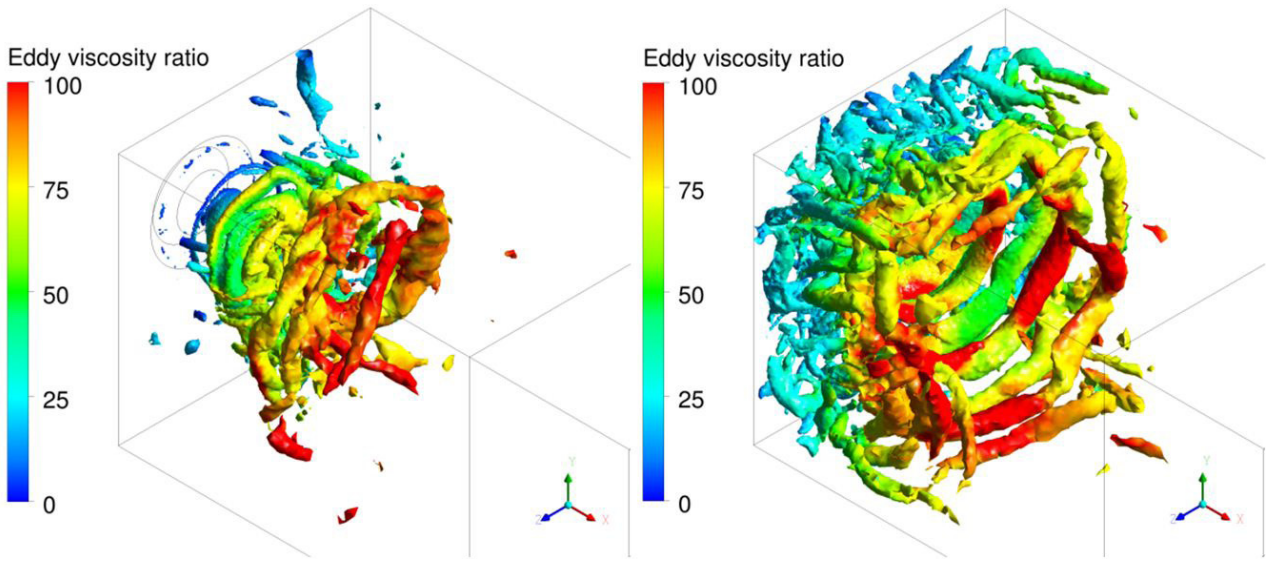

Figure 13. *SAS solution for ITS combustion chamber, isosurface $\Omega^2-S^2=10^7\ s^{-2}$. Left: nonreacting flow; right: reacting flow*

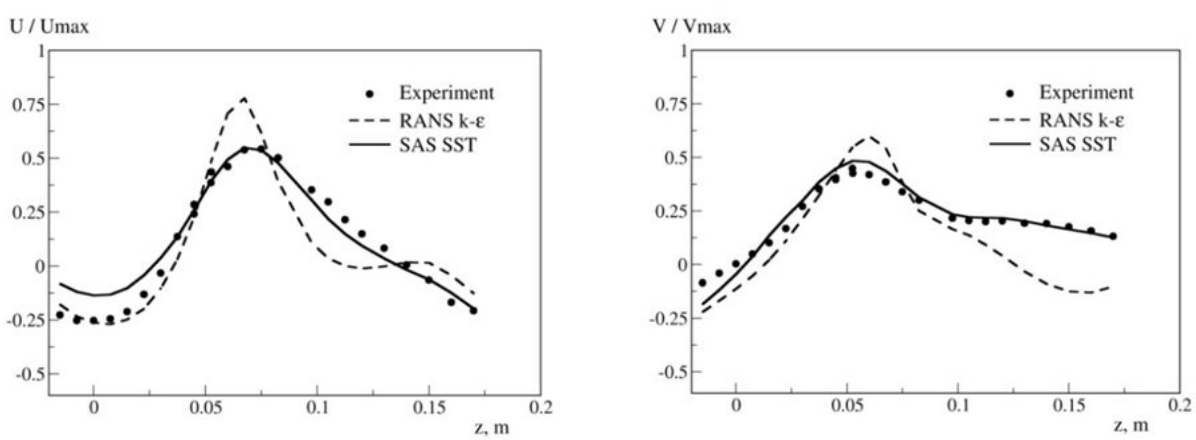

Figure 14. *Nonreacting flow velocity profiles at the axial distance from the inlet x=138 mm. Left: axial velocity; right: tangential velocity*

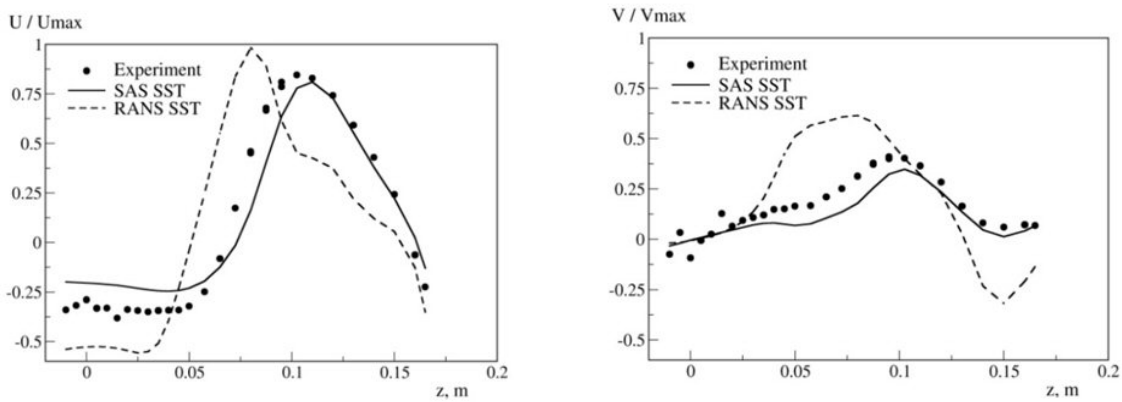

Figure 15. *Reacting flow velocity profiles at x=103 mm. Left: axial velocity; right: tangential velocity*

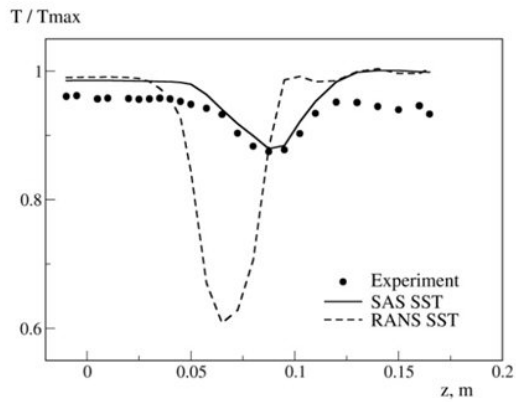

Figure 16. *Reacting flow temperature profile at x=103 mm*

Air flow past a 3-D rectangular shallow cavity was calculated to test the SAS model's ability to predict correct spectral information for acoustics applications: the cavity geometry and flow conditions corresponding to the M219 experimental test case of Henshaw (2000). The experiment investigates noise generation due to turbulent structures forming from the cavity's front lip and interacting with cavity walls.

Figure 17 shows turbulent structures produced by the SST-SAS model (iso-surface Q-criterion). The power spectral density (PSD) of the transient pressure signals calculated and measured by sensors on the cavity bottom near the leading and the downstream wall, respectively, is plotted in Figure 18. These plots show that PSD levels are captured in good agreement with the data. Similar agreement was achieved for other experimental locations (not shown here).

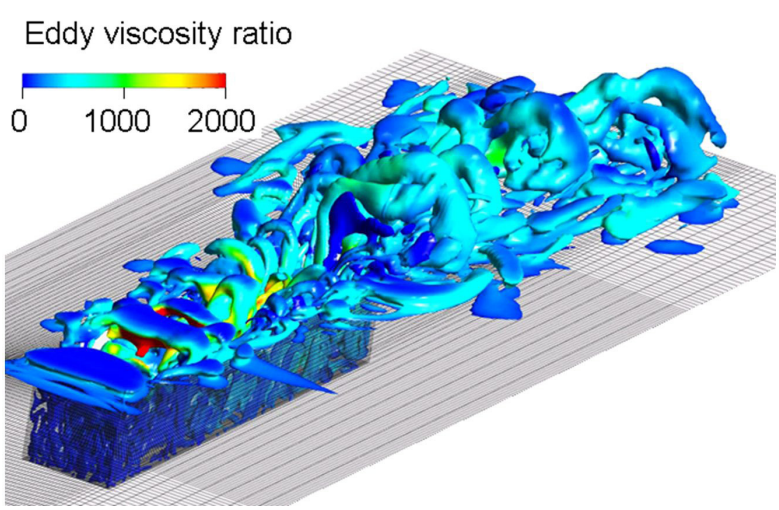

Figure 17. *Resolved turbulent structures for cavity flow: iso-surface Ω^2-S^2=5 • 105 s^{-2}*

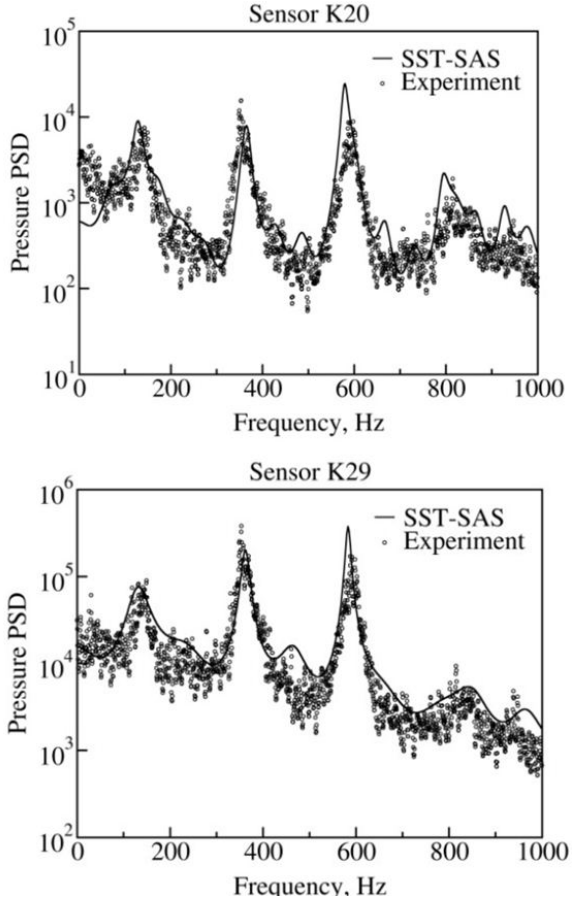

Figure 18. *Power spectral density of transient wall pressure signals on the cavity bottom; top: sensor K20 located close to front wall; bottom: sensor K29 located close to rear wall*

In Egorov et al. (2010), the SAS model is described in detail and is applied to a wide variety of generic and industrial-like flows.

ZONAL RANS-LES MODELS

Hybrid models like DES and SAS rely on flow instabilities to generate turbulent structures in large separated regions without the explicit introduction of unsteadiness through the boundary conditions. However, there are situations in which such instabilities are not present or are not reliable to serve this purpose. In such cases, it is desirable to apply RANS and LES models in predefined zones and provide clearly defined interfaces between them. At these interfaces, the modeled turbulent kinetic energy from the upstream RANS model is converted explicitly to resolved scales at an internal boundary to the LES zone. The LES zone can then be limited to the region of interest for which unsteady results are required.

There are numerous zonal RANS-LES concepts, and it is not possible to cover them all. The following results, therefore, are limited to the methods implemented in ANSYS® FLUENT® and ANYS CFX technologies. These approaches have been selected since they appear most attractive from an industrial CFD perspective. [Note that the references provide general concepts — the model formulation has since evolved]. In ANSYS FLUENT, an embedded-LES (ELES) option has been implemented (Cokljat et al 2009). It allows the user to prespecify RANS and LES zones in a single CFD simulation. At the RANS-LES interface, the modeled turbulence from the RANS model is converted into resolved turbulence using the methods previously available for this purpose at inlets. ELES allows the selection of virtually all RANS models in the RANS domain and algebraic LES models in the LES region.

In ANSYS CFX, a newly developed method based on forcing terms is available (Menter et al. 2009). It also allows the user to define RANS and LES regions in the domain. Inside the LES region, the eddy viscosity of the RANS model is forced down to a preselected LES formulation. At the interface, forcing terms in the momentum equations generate the turbulent content.

Both methods can be used for a wide variation of applications, and they allow a flexible and controlled interaction of RANS and LES zones. Figure 19 shows the application of ELES to a channel flow. The front portion of the channel is covered by a RANS model. The RANS-LES interface uses the vortex method (Mathey et al. 2006) to convert modeled turbulence to resolved synthetic turbulence and the WALE LES model to provide an LES eddy viscosity. Downstream, the method switches back to RANS.

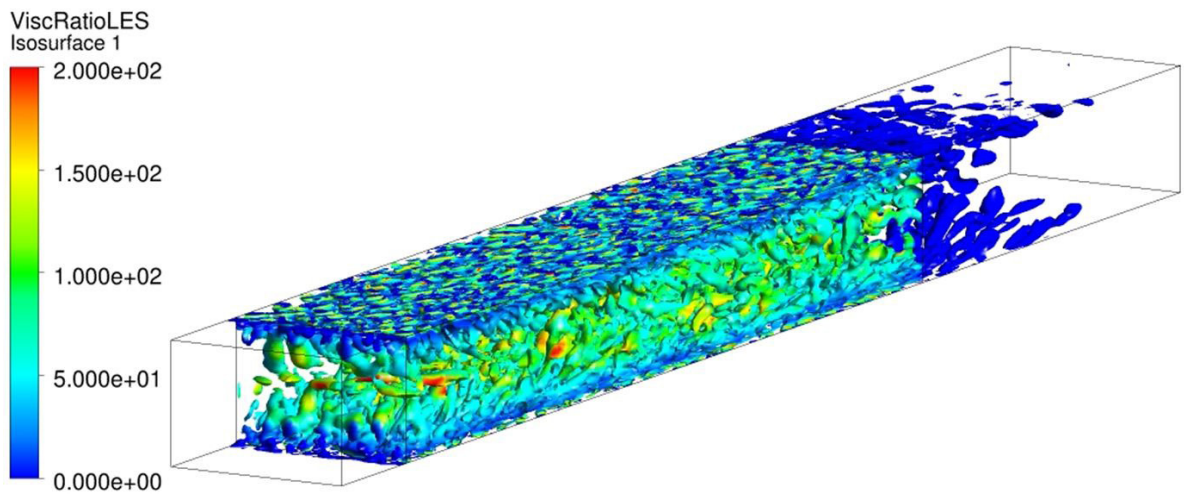

Figure 19. *Channel flow: viscosity ratio on iso-surfaces of Q-criterion (-500)*

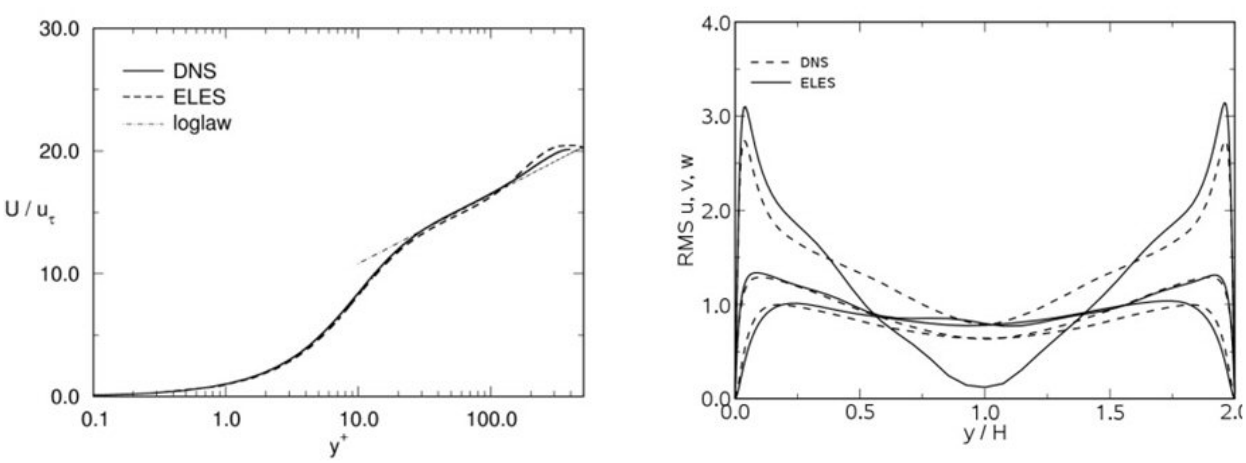

Figure 20. *Fully developed channel flow. Left: mean velocity values inside LES zone; right rms values inside LES zone at x=1.5 +1.5*Π

Figure 20 shows a comparison of LES results inside the embedded region with DNS data of Moser et al. (1998) both for the mean flow profile and turbulence RMS values. The agreement is quite close, considering the limited length of the LES zone.

WALL-MODELED LES

A relatively recent approach to address LES limitations for high Re number boundary layers is termed wall-modeled LES (WMLES). It is based on the concept of covering the inner portion of the boundary layer by RANS and the outer portion by LES. This avoids the very high resolution requirements of LES in the inner wall layer. A very simple and promising approach to WMLES has been proposed by Shur et al. (2008). It is based on a reformulation of the length scale used in the LES zone and by blending it with the mixing length (RANS) model in the inner part of the boundary layer.

Figure 21 shows a series of simulations for periodic channel flows with increasing Reynolds number using ANSYS FLUENT. The grids used for these simulations are given in Table 2. It is well known that the use of hybrid models without further provisions will result in a strong log-layer mismatch and a corresponding error in the wall shear stress (Spalart et al. 2006). Figure 21 shows that the log-layer mismatch can be reduced to a relatively small shift at the RANS-LES interface, resulting in a high quality solution even at very high Re numbers.

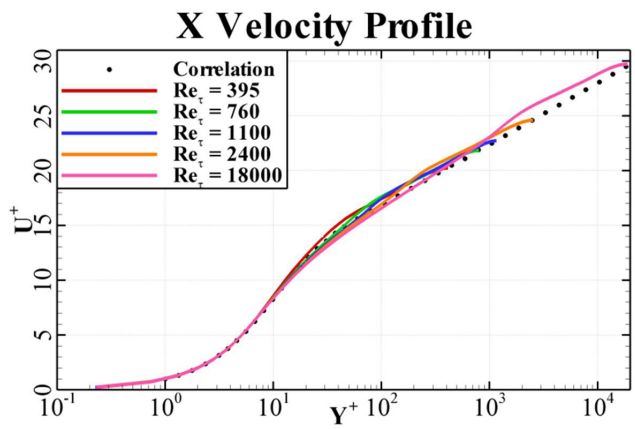

Figure 21. *Velocity profiles in logarithmic scale for periodic channel flow using WMLES for various Reynolds numbers*

The simulations were carried out on grids with the characteristics given in Table 2. The domain size was LX=16h, LY=2h, LZ=3h (h being half the channel height; this corresponds approximately to the boundary layer thickness for wall boundary layers). The main characteristics of WMLES are clearly visible from Table 2, the nondimensional values for ΔX^+ and ΔZ^+ are far beyond the limits of standard LES methods (ΔX^+=40, ΔZ^+=20). For WMLES, one only has to ensure a minimum number of cells per boundary layer volume h x h x h. In the current formulation, the minimum resolution per boundary layer volume is of the order of 10*x*40*x*20 cells (streamwise, normal and spanwise).

Re_τ	Cells	Nodes Number	ΔX^+ Number	ΔY^+	ΔZ^+
395	384 000	81×81×61	40.0	0.2 ÷ 30	20.0
395	1 764 000	141×141×91	26.6	0.2 ÷ 20	13.3
760	480 000	81×101×61	76.9	0.2 ÷ 30	38.5
1100	480 000	81×101×61	111.4	0.2 ÷ 30	55.7
2400	528 000	81×111×61	243.0	0.2 ÷ 30	121.5
18000	624 000	81×131×61	1822.7	0.2 ÷ 30	911.4

Table 2. *Grids for periodic channel flow at different Reynolds number using WMLES*

The grid for the boundary layer test case has the following parameters, Table 3:

Re_{Θ}	Cells	Nodes Number	ΔX^+ Number	ΔY^+	ΔZ^+
1000/10000	1 050 000	251×71×62	16	0.2 ÷ 80	8

Table 3: *Grids for periodic channel flow at different Reynolds number using WMLES*

Figure 22 shows the turbulent structures for a wall boundary layer flow again using the WMLES option. The outer part is covered by LES and the near-wall part by RANS. The flow is computed with ANSYS FLUENT, and the turbulence at the inlet is generated by the vortex method. The turbulence is well maintained as can be seen from Figure 23 in which the wall shear stress is displayed relative to the RANS solution provided at the inlet. The WMLES recovers quickly from synthetic turbulence and maintains a proper turbulence further downstream.

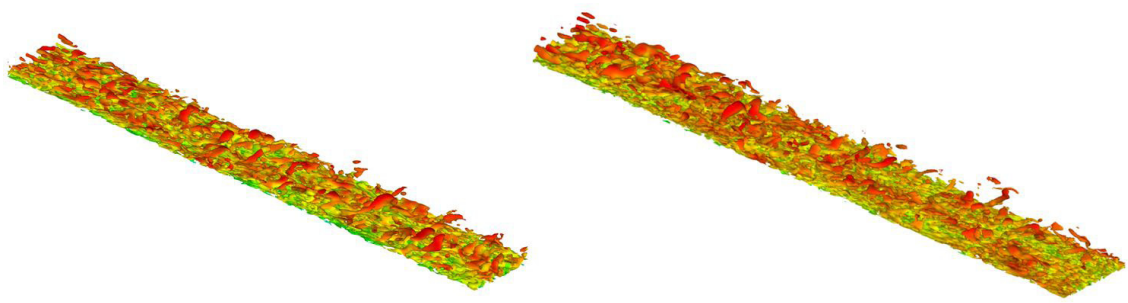

Figure 22. *Turbulence structures for wall boundary layer flow using the WMLES option and vortex method to generate synthetic turbulence at the inlet; right: Re_{Θ}=1000; left: Re_{Θ}=10000*

Figure 23 shows the wall shear stress distributions for both Reynolds numbers. The inlet condition is provided from by the vortex method, which converts a RANS profile from the SST-RANS model into synthetic turbulence.

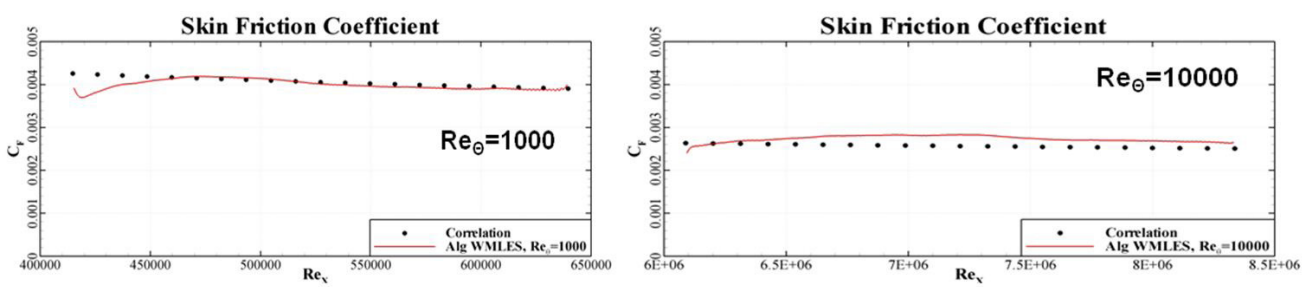

Figure 23. *Wall shear stress coefficient for wall boundary layer flow using WMLES option and vortex method to generate synthetic turbulence at the inlet; right: Re_{Θ}=1000; left: Re_{Θ}=10000*

WMLES is still substantially more computationally expensive than RANS. However, it avoids the excessive Re number scaling of classical LES and allows the simulation of limited components of technical devices for which RANS models simulations are not of sufficient accuracy.

A more challenging test case for ELES in combination with WMLES has been computed within the EU project ATAAC. It is the flow over a hump with a relatively large separation zone on the leeward side. Figure 24 shows the experimental setup (Greenblatt et al. 2005).

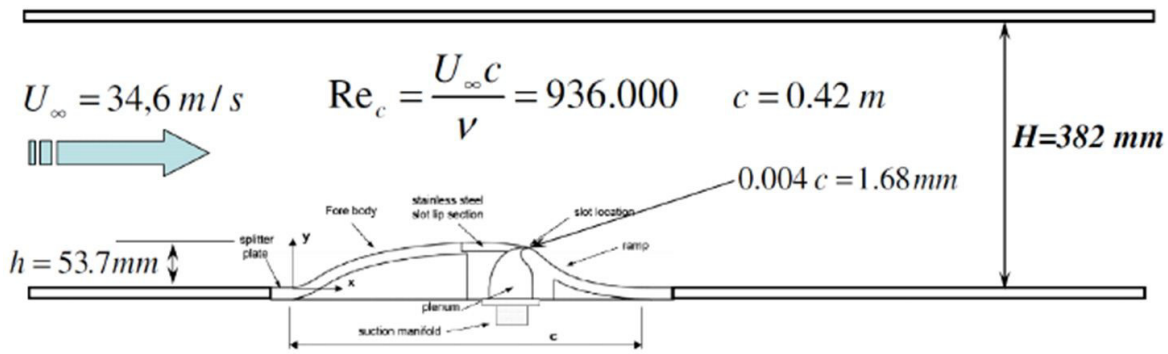

Figure 24. *Experimental setup up for NASA hump flow experiment*

The flow has been computed with ANSYS FLUENT 13.0 using the SST model in the RANS zone, vortex method at the RANS-LES interface and WMLES option in the LES zone.

The grid for the test case can be seen in Figure 25 together with a visualization of turbulent structures in the LES zone. The grid in the LES zone consists of 200x100x100 cells and is designed to provide 10x40x20 cells in streamwise, normal and spanwise directions per boundary layer volume. The RANS grid is much coarser, especially in the spanwise direction. The momentum thickness Reynolds number at the inlet to the LES domain is relatively high (Re_Θ=7000).

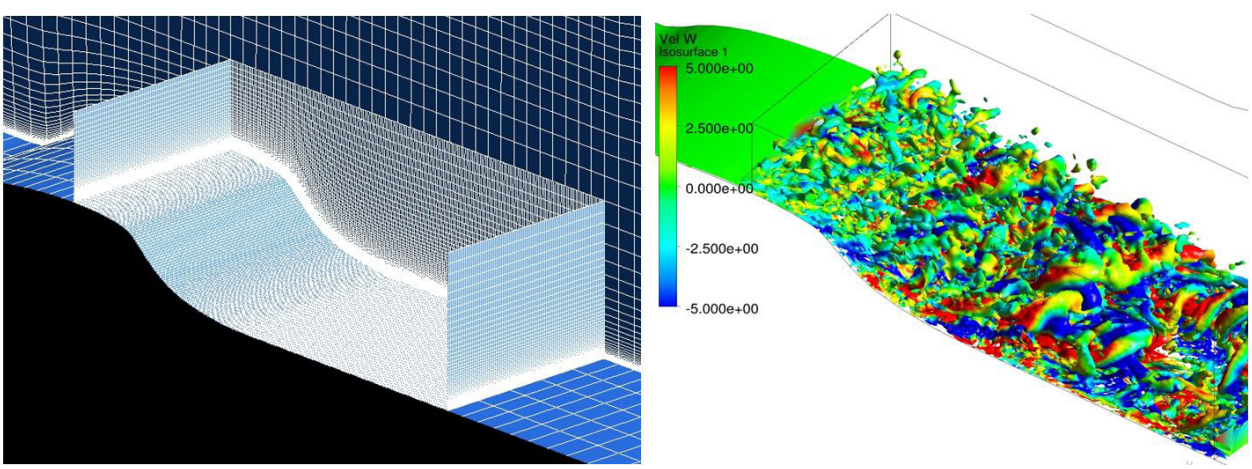

Figure 25. *Left: grid for NASA hump simulation; right: turbulent structures in LES domain (color spanwise velocity component)*

Figure 26 shows the wall shear stress and wall pressure coefficient for these simulations. The combination with the WMLES formulation provides a close agreement even with the very sensitive wall shear stress coefficient, cf. From the pressure coefficient, cp, the length of the separation zone is predicted correctly. One of the more interesting observations from the study resulted from the application of the standard WALE LES model inside the LES zone. Due to the high Re number, the WALE model is not able to carry the turbulent boundary layer. It separates immediately after the RANS-LES interface and overpredicts the separation length. This clearly illustrates the advantages of WMLES for higher Re-number wall-bounded flows.

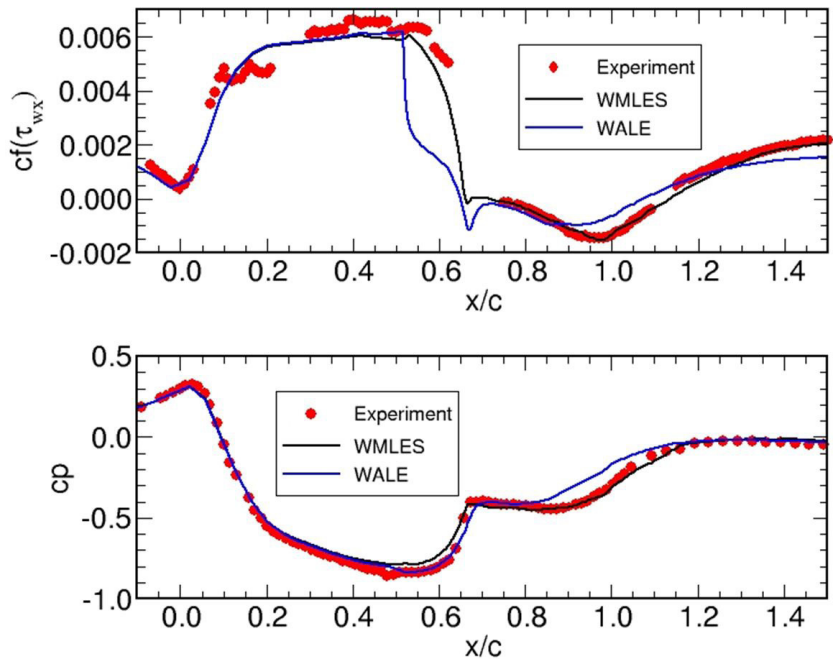

Figure 26. *Wall shear stress, cf, and wall pressure coefficients, cp, for NASA hump flow simulations: comparison of WMLES and WALE LES method in LES domain*

Summary

Turbulence modeling is and will remain one of the driving technologies in CFD. The wide range of industrial CFD code applications demands a balanced model offering, one that allows the inclusion of all relevant physical effects while providing solutions with available computing power and within acceptable turn-around times for industrial users. For many applications, RANS models are and will remain the optimal choice in terms of a proper balance of accuracy and computational resources. The goal of further improvements is the inclusion of additional effects such as turbulence anisotropy without compromising the current calibration level of the models.

Modeling laminar–turbulent transition will also remain an area of active research and software development; the author's organization will continue developing model formulation in this sector. It is anticipated that the ever-increasing demand for accuracy will reveal that many more CFD applications can benefit from taking the laminar–turbulent transition process into account.

The main thrust in industrial CFD will be in the area of scale-resolving simulation (SRS) models. Industrial CFD codes will have to offer a wide range of the most-advanced model formulations, ranging from SAS and DES all the way to zonal methods with interface conditions. Finally, the challenge of computing high Re number flows with wall-modeled LES will continue to be a focal point of future research activities.

ACKNOWLEDGMENTS

Some of the results in this paper were produced during the European Research Projects Flomania DESIDER and ATAAC and have been funded by the European Union. The author thanks his colleagues Yuri Egorov, Robin Langtry (now at The Boeing Company), Richard Lechner and Pavel Smirnov (now at ANSYS) and Mikhail Gritskevich from NTS, who performed the computations shown in this article.

References

Brodersen, O., and Stürmer, A., (2001), "Drag Prediction of Engine–Airframe Interference Effects Using Unstructured Navier-Stokes Calculations," AIAA Paper 2001-2414.

Cokljat, D., Caradi, D., Link, G., Lechner, R. and Menter, F.R. (2009), "Embedded LES Methodology for General-Purpose CFD Solvers." Proc. Turbulent Shear Flow Phenomena, Proc. 6th Int. Symp. Turbulence and Shear Flow Phenomena, Seoul, Korea, 22-24 June 2009, 1191-1196.

Coles, D., and Wadcock, A.J. (1979): "A Flying-Hot-Wire Study of Two-Dimensional Mean Flow Past an NACA 4412 Airfoil at Maximum Lift," AIAA J. Vol. 17, No. 4, pp 321-328.

Dorney, D.J., Lake, J.P., King, P.L. and Ashpis, D.E., (2000), "Experimental and Numerical Investigation of Losses in Low-Pressure Turbine Blade Rows," AIAA Paper AIAA-2000-0737, Reno, NV.

Durbin, P.A. (1995), "Separated Flow Computations with the k-ε-v2 Model," AIAA J. 33, pp. 659-664.

Durbin, P.A. and Reif, B.A., (2001), "*Statistical Theory and Modeling for Turbulent Flows*," John Wiley & Sons.

Egorov, Y, Menter, F.R. and Cokljat D., (2009), "Scale-Adaptive Simulation Method for Unsteady Flow Predictions. Part 2: Application to Aerodynamic Flows," Journal Flow Turbulence and Combustion, Vol. 85, No. 1, pp. 139-165.

Esch T. and Menter, F.R., (2003), "Heat Transfer Predictions Based on Two-Equation Turbulence Models with Advanced Wall Treatment," Turbul. Heat Mass Transf. 4, pp. 6333-640.

Fröhlich J., Mellen C.P., Rodi W., Temmerman L., and Leschziner M.A. (2005), "Highly-Resolved Large Eddy Simulations of Separated Flow in a Channel with Streamwise Periodic Constrictions," J. Fluid Mech., 526:19-66.

Fröhlich J. and von Terzi, D. (2008), "Hybrid LES/RANS Methods for Simulation of Turbulent Flows," Progress in Aerospace Sciences, Vol. 44, Issue 5, pp 349-377, 2008.

Greenblatt, D., Paschal, K. B., Yao, C.-S. and Harris, J. (2005): "A Separation Control CFD Validation Test Case, Part 2: Zero Efflux Oscillatory Blowing." AIAA Paper No. 2005-0485 (also in AIAA Journal, Vol. 44, No. 12, 2006, pp. 2831-2845).

Haase, W., Braza, M. and Revell A., (2009), "DESider – A European Effort on Hybrid RANS-LES Modeling," Notes on Numerical Fluid Mechanics and Multidisciplinary Design, Vol. 103, Springer.

Henshaw, M. J. de C. (2000): "M219 cavity case, In: "Verification and Validation Data for Computational Unsteady Aerodynamics," Tech. Rep. RTO-TR-26, AC/323/(AVT) TP/19, pp. 473-480.

Huang, J., Corke, T.C., Thomas, F.O., (2003), "Plasma Actuators for Separation Control of Low Pressure Turbine Blades," AIAA Paper No. AIAA-2003-1027.

Kalitzin, G., Medic, G., Iaccarino, G., Durbin, P., (2005), “Near-wall Behaviour of RANS Turbulence Models and Implications for Wall Functions,” J. Comput. Phys. 204, 265–291.

Kim S.E., Cokljat D. and Choudhury D. (2002), “A Pragmatic Near-Wall Treatment for Turbulent Flows and Heat Transfer,” (Paper presented at poster session), 5th ASME-ISHMT Heat and Mass Transfer Conference, 3-5 January, Calcutta, India.

Klausmeyer, S.M. and Lin, J.C., (1997), “Comparative Results From a CFD Challenge Over a 2D Three-Element High-Lift Airfoil,” NASA Technical Memorandum 112858.

Langtry, R., Kuntz, M. and Menter, F.R., (2004), “Drag Prediction of Engine-Airframe Interference Effects with CFX-5,” AIAA Paper 2004-0392, Reno.

Langtry R. and Menter, F.R., (2009), “A Correlation-Based Transition Model using Local Variables for Unstructured Parallelized CFD Codes,” AIAA Journal, Vol. 47, No.12.

Laschka, B., Ranke and H., Breitsamter, C., (1995): “Application of unsteady measurement techniques to vortical and separated flows,” Z. Flugwiss. Weltraumforsch. 19, 90-108.

Malan, P., Suluksna, K., and Juntasaro, E., (2009), “Calibrating the γ-Re_{Θ} Transition Model for Commercial CFD,” AIAA Paper-2009-1142, Orlando 2009.

Mathey F., Cokljat D., Bertoglio J.P. and Sergent E. (2006), “Specification of LES Inlet Boundary Condition Using Vortex Method,” Progress in Computational Fluid Dynamics, Vol. 6, No 1-3, pp. 58-67.

Mayle, R.E., (1991), “The Role of Laminar-Turbulent Transition in Gas Turbine Engines,” Journal of Turbomachinery, Vol. 113, pp. 509-537.

Menter, F.R. (1992), “Influence of Freestream Values on k-ω Turbulence Model Predictions,” AIAA-Journal, Vol. 30, No.6, pp. 1657-1659.

Menter, F.R., (1994), “Two-Equation Eddy-Viscosity Turbulence Models for Engineering Applications,” AIAA-Journal, 32(8), pp. 269-289, 1994.

Menter, F.R., Esch, T.E., (2001), “Elements of Industrial Heat Transfer Predictions,” Keynote lecture at the 16th Brazilian Congress of Mechanical Engineering, Brazil.

Menter F.R. and Kuntz M., (2002), “Adaptation of Eddy-Viscosity Turbulence Models to Unsteady Separated Flow Behind Vehicles.” Proc. Conf. The Aerodynamics of Heavy Vehicles: Trucks, Buses and Trains, Asilomar, Ca, 2002.

Menter, F.R., Langtry, R., Völker, S., (2006), “Transition Modeling for General Purpose Codes,” Journal Flow Turbulence and Combustion, Vol. 77, No. 1-4, pp. 277-303.

Menter F.R., (2009), “Review of the Shear-Stress Transport Turbulence Model Experience from an Industrial Perspective,” Int. J. of Comp. Fluid Dynamics, Vol. 23, No. 4, pp. 305-316.

Menter, F.R., Garbaruk, A.V. and Egorov, Y., (2009), “Explicit Algebraic Reynolds Stress Models for Anisotropic Wall-Bounded Flows,” Invited Lecture: EUCASS – 3rd European Conference for Aero-Space Sciences, July 6-9th 2009 Versailles.

Menter F.R., Garbaruk A., Smirnov P., (2009), ”Scale Adaptive Simulation with Artificial Forcing,” Proc. 3rd Symposium on Hybrid RANS-LES Methods, Gdansk.

Menter, F.R. and Egorov, Y., (2010), “Scale-Adaptive Simulation Method for Unsteady Flow Predictions. Part 1: Theory and Model Description,” Journal Flow Turbulence and Combustion, Vol. 85, No. 1, pp 113-138.

Moser R.D., Kim J. And Mansour N.N., (1998), “DNS of Turbulent Channel Flow up to Re_tau=590,” Phys. Fluids, Vol11, pp. 943-945.

Pope, S.B. (1999), “A Perspective on Turbulence Modeling,” in Modeling Complex Turbulent Flows Eds. M.D. Salas, J.N. Hefner and L. Sakell, Kluwer, pp.53-67.

Popovac, M. and Hanjalic, K., (2007), “Compound Wall Treatment for RANS Computation of Complex Turbulent Flows and Heat Transfer,” J. Flow Turbulence and Combustion, Vol. 78, No. 2, pp. 177-202.

Roache, P.J., (1989), “Verification and Validation in Computational Science and Engineering,” Hermosa Publishers.

Rodi, W. (1976), “A New Algebraic Relation for Calculating the Reynolds Stresses,” Z. Angew. Math. Mech, Vol. 56, pp 219-221.

Rodi, W., (1991), “Experience with Two-Layer Models Combining the k-epsilon Model with a One-Equation Model Near the Wall,” AIAA, Aerospace Sciences Meeting, 29th, Reno, NV, Jan. 7-10, 1991. 13 p.

Schildmacher, K.-U., Koch, R., Wittig, S., Krebs, W. and Hoffmann, S., (2000): “Experimental Investigations of the Temporal Air-Fuel Mixing Fluctuations and Cold Flow Instabilities of a Premixing Gas Turbine Burner,” ASME Paper 2000-GT-0084.

Shur, M.L., Spalart P.R., Strelets M. and Travin A., (2008), “A Hybrid RANS-LES Approach with Delayed-DES and Wall-Modelled LES Capabilities.” Int. J. Heat Fluid Flow International Journal of Heat and Fluid Flow, Vol. 29, No 6, pp. 1638-1649.

Smagorinsky, J. (1963), “General Circulation Experiments with the Primitive Equations, i. the basic experiment. Monthly Weather Review,” 91: pp. 99-164, 1963.

Spalart P. R., (2000), “Strategies for Turbulence Modeling and Simulations,” Int. J. Heat Fluid Flow, 21, pp. 252-263.

Spalart, P., Deck, S., Shur, M., Squires, K., Strelets, M., Travin, A., (2006), “A New Version of Detached Eddy Simulation, Resistant to Ambiguous Grid Densities,” Journal of Theoretical and Computational Fluid Dynamics 20, pp. 181–195.

Strelets, M., (2001), “Detached Eddy Simulation of Massively Separated Flows,” AIAA Paper 2001-0879.

Suzen, Y.B., Huang, P.G., Hultgren, L.S., Ashpis, D.E., (2003), “Predictions of Separated and Transitional Boundary Layers Under Low-Pressure Turbine Airfoil Conditions Using an Intermittency Transport Equation,” Journal of Turbomachinery, Vol. 125, No. 3, July 2003, pp. 455-464.

Temmerman L. and Leschziner, M.A.(2001): “Large Eddy Simulation of Separated Flow in a Streamwise Periodic Channel Constriction,” Proceedings, 2nd Symp. on Turbulence and Shear-Flow Phenomena, Stockholm.

Walters K. Cokljat, D., (2008), “A Three-Equation Eddy-Viscosity Model for Reynolds-Averaged Navier–Stokes Simulations of Transitional Flow,” J. Fluids Eng., Volume 130, Issue 12.

Wallin, S. and Johansson, A.V., (2000), ”An Explicit Algebraic Reynolds Stress Model for Incompressible and Compressible Turbulent Flows,” J. Fluid Mech., 403, pp. 89–132.

Widenhorn, A., Noll, B, and Aigner, M. (2009): “Numerical Study of a Non-Reacting Turbulent Flow in a Turbine Model Combustor,” AIAA Paper 2009-647, Orlando Florida.

Wilcox, D.C. (2006), *Turbulence Modeling for CFD*, 3rd Ed., DCW Industries, Inc.

www.ansys.com

ANSYS, Inc.
Southpointe
275 Technology Drive
Canonsburg, PA 15317
U.S.A.
724.746.3304
ansysinfo@ansys.com

Toll Free U.S.A./Canada:
1.866.267.9724
Toll Free Mexico:
001.866.267.9724
Europe:
44.870.010.4456
eu.sales@ansys.com

© 2011 ANSYS, Inc. All Rights Reserved.